JCTC Journal of Chemical Theory and Computation

Article

pubs.acs.org/JCTC

Analytic Gradient for Density Functional Theory Based on the Fragment Molecular Orbital Method

Kurt R. Brorsen,[†] Federico Zahariev,[†] Hiroya Nakata,[‡,§,▽] Dmitri G. Fedorov,[⊥] and Mark S. Gordon*[,†]

[†]Ames Laboratory, U.S. Department of Energy (US-DOE), Department of Chemistry, Iowa State University, Ames, Iowa 50011, United States

[‡]Department of Biomolecular Engineering, Tokyo Institute of Technology, 4259 Nagatsuta-cho, Midori-ku, Kanagawa, Yokohama 226-8501, Japan

[§]Nakamura Laboratory, RIKEN Research Cluster for Innovation, 2-1 Hirosawa, Wako, Saitama 351-0198, Japan

[▽]Japan Society for the Promotion of Science, Kojimachi Business Center Building, 5-3-1 Kojimachi, Chiyoda-ku, Tokyo 102-0083, Japan

[⊥]NRI, National Institute of Advanced Industrial Science and Technology (AIST), 1-1-1 Umezono, Tsukuba, Ibaraki 305-8568, Japan

ABSTRACT: The equations for the response terms for the fragment molecular orbital (FMO) method interfaced with the density functional theory (DFT) gradient are derived and implemented. Compared to the previous FMO−DFT gradient, which lacks response terms, the FMO−DFT analytic gradient has improved accuracy for a variety of functionals, when compared to numerical gradients. The FMO−DFT gradient agrees with the fully *ab initio* DFT gradient in which no fragmentation is performed, while reducing the nonlinear scaling associated with standard DFT. Solving for the response terms requires the solution of the coupled perturbed Kohn−Sham (CPKS) equations, where the CPKS equations are solved through a decoupled Z-vector procedure called the self-consistent Z-vector method. FMO−DFT is a nonvariational method and the FMO−DFT gradient is unique compared to standard DFT gradients in that the FMO−DFT gradient requires terms from both DFT and time-dependent density functional theory (TDDFT) theories.

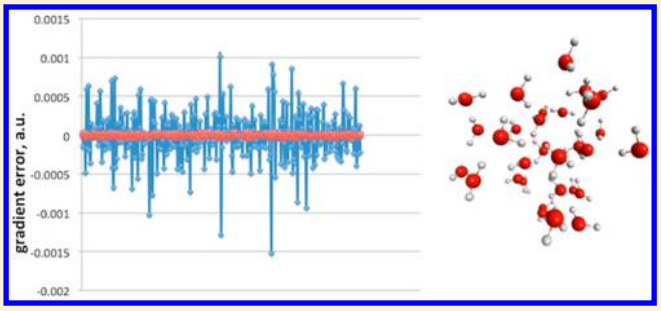

1. INTRODUCTION

The fragment molecular orbital (FMO) method[1] is one of many techniques[2−11] that seek to reduce the scaling[12] of standard quantum chemical methods by fragmentation. FMO has been applied to many biological[13−15] and inorganic systems.[16,17] Since electron correlation plays an important role in many systems of chemical interest, the FMO method was interfaced with density functional theory (DFT),[18] including an energy gradient.[19] FMO−DFT is similar to the FMO−RHF model except that the Kohn−Sham equations are solved instead of the Hartree−Fock equations. In the FMO prescription,[20−22] the individual fragments (monomers) are iterated to self-consistency.[23] However, if pairs of fragments (dimers) are included explicitly (as in the FMO2 level of theory), the dimers are not iterated to self-consistency. Because the dimer calculations are not iterated to self-consistency, with respect to the embedding potential of other fragments, it is necessary, even for first-order derivatives, to include response terms that arise from the derivatives of the dimer molecular orbital coefficients, with respect to the nuclear coordinates of atoms in other fragments.[24,25] Similar to other FMO gradient implementations at the time,[24−27] response terms for the FMO−DFT gradient were not included, because of the complexity of solving for the response terms. The authors assumed that the contribution of the response terms to the gradient would be small and, therefore, could be ignored in most circumstances. However, the inclusion of response terms improves the efficiency of geometry optimizations, while, for FMO molecular dynamics (MD) simulatons,[28−30] the neglect of the response terms in the energy gradient results in poor energy conservation in the microcanonical ensemble.[28] In addition, the error in the analytic gradient prevents the implementation of semianalytic Hessians (i.e., finite differences of analytic gradients). The lack of semianalytic Hessians means that the FMO method must use fully numerical Hessians. Fully numerical Hessians can be computationally intense and are prone to error, thereby limiting the applicability of FMO for finding transition states and the verification of potential energy minima.

Because of the shortcomings in the original FMO gradient, the analytic FMO restricted Hartree−Fock (RHF) gradient, including response terms, was derived and implemented.[25] The response terms were included through the self-consisted Z-Vector (SCZV) method. The Z-Vector[31−33] is calculated in the Z-vector "field" of the other fragments. Since the derivation

Received: May 23, 2014
Published: October 30, 2014

   dx.doi.org/10.1021/ct500808p | *J. Chem. Theory Comput.* 2014, 10, 5297−5307

of the FMO-RHF response terms, further improvements to the FMO gradient have followed, including extensions to unrestricted Hartree−Fock (UHF),[34] second-order Møller−Plesset perturbation theory (MP2),[35] and the electrostatic point charge (ESP-PC) approximation.[36,37] The analytic energy gradient has also been interfaced with the polarizable continuum model (PCM),[38] and the effective fragment potential (EFP).[39] In addition, FMO analytic Hessians have been implemented for both RHF and unrestricted HF (UHF).[40]

It has been demonstrated that the improved FMO−RHF gradient eliminates the lack of energy conservation for FMO-MD simulations.[30] In the present work, the derivation of the fully analytic closed shell FMO−DFT gradient is presented and the implementation of the method is discussed.

Because the Kohn−Sham and coupled perturbed Kohn−Sham (CPKS) equations[41] are similar to the Hartree−Fock and coupled perturbed Hartree−Fock equations, the derivation and implementation presented in the present study closely follows that of the FMO−RHF analytic gradient.[25]

While the FMO−DFT derivation presented below is similar to that of FMO−RHF, the derivation is unique when compared to other DFT gradients. Because the FMO2−DFT method is not variational, first-order derivatives require higher order functional derivatives than do standard DFT gradients. The higher-order functional derivatives normally arise in time-dependent density functional theory (TDDFT) calculations; therefore, the FMO−DFT gradient employs both DFT and TDDFT.

2. ANALYTIC GRADIENT FOR FMO−DFT

The FMO2-DFT energy expansion is

$$E = \sum_{I}^{N} E'_I + \sum_{I>J}^{N} (E'_{IJ} - E'_I - E'_J) + \sum_{I>J}^{N} \mathrm{Tr}(\Delta\mathbf{D}^{IJ}\mathbf{V}^{IJ}) \tag{1}$$

E'_X is the internal fragment energy of monomer ($X = I$) or dimer ($X = IJ$), $\mathbf{V}^{IJ}$ is the matrix of the electrostatic potential for dimer IJ, and $\Delta\mathbf{D}^{IJ}$ is the dimer density difference matrix, which is defined as

$$\Delta\mathbf{D}^{IJ} = \mathbf{D}^{IJ} - (\mathbf{D}^{I} \oplus \mathbf{D}^{J}) \tag{2}$$

In eq 2, $\mathbf{D}^{\mathbf{X}}$ is the density of fragment X, where the density of each monomer is obtained with respect to the electrostatic potential of all other monomers. The internal fragment energy is defined as

$$E'_X = \sum_{\mu\nu\in X} D^X_{\mu\nu} h^X_{\mu\nu} + \frac{1}{2}\sum_{\mu\nu\lambda\sigma\in X}\left[D^X_{\mu\nu}D^X_{\lambda\sigma} - \frac{c_x}{2}D^X_{\mu\lambda}D^X_{\nu\sigma}\right](\mu\nu|\lambda\sigma) + E^X_{xc} + E^X_{NR} \tag{3}$$

$h^X_{\mu\nu}$ is the one-electron Hamiltonian of monomer or dimer X, c_x is the scaling factor for hybrid functionals, and $(\mu\nu|\lambda\sigma)$ is a two-electron integral in the atomic orbital basis. In the study, Roman ($ijkl\cdots$) and Greek ($\mu\nu\lambda\sigma\cdots$) indices denote the molecular orbitals and atomic orbitals, respectively. The nuclear repulsion energy E^X_{NR} is defined as

$$E^X_{NR} = \sum_{\mathrm{B}\in X}\sum_{\mathrm{A}(\in X)>\mathrm{B}} \frac{Z_\mathrm{A}Z_\mathrm{B}}{R_{\mathrm{AB}}} \tag{4}$$

Z_A is the nuclear charge of atom A, and R_{AB} is the distance between atoms A and B. E^X_{xc} is the exchange-correlation energy. The exchange-correlation energy $E^X_{xc}[\rho^X]$ is a functional of the density of fragment X,

$$\rho^X(\vec{r}) = \sum_{\mu\nu\in X} D^X_{\mu\nu}\phi^X_\mu(\vec{r})\phi^X_\nu(\vec{r}) \tag{5}$$

where $\phi^X_\mu(\vec{r})$ are atomic orbitals in fragment X.

If fragmentation occurs across a covalent bond, the hybrid orbital projection (HOP) contribution[42]

$$\sum_{i\in X}^{\mathrm{occ}} 2\langle i|\hat{P}^X|i\rangle = \sum_{\mu\nu\in X} D^X_{\mu\nu}P^X_{\mu\nu} \tag{6}$$

must be added to E'_X; $\hat{P}^X$ is the hybrid projection operator,

$$\hat{P}^X = \sum_{k\in X} B_k|\theta_k\rangle\langle\theta_k| \tag{7}$$

$|\theta_K\rangle$ is the hybrid orbital and B_k is a constant. $P^X_{\mu\nu}$ is the matrix element of the hybrid projection operator,

$$P^X_{\mu\nu} = \langle\mu|\hat{P}^X|\nu\rangle \tag{8}$$

The matrix V in eq 1 is formed from one- and two-electron contributions:

$$V^X_{\mu\nu} = \sum_{K\neq X}(u^K_{\mu\nu} + v^K_{\mu\nu}) \tag{9}$$

The one-electron and two-electron parts are defined in eqs 10 and 11, respectively.

$$u^K_{\mu\nu} = \sum_{\mathrm{A}\in\mathrm{K}}\langle\mu|\frac{-Z_\mathrm{A}}{|r-R_\mathrm{A}|}|\nu\rangle \tag{10}$$

$$v^K_{\mu\nu} = \sum_{\lambda\sigma\in\mathrm{K}} D^\mathrm{K}_{\lambda\sigma}(\mu\nu|\lambda\sigma) \tag{11}$$

Calculation of the two-electron terms is expensive; therefore, in most FMO calculations, a cutoff value is specified such that for monomers separated by a distance greater than the cutoff value, the two-electron term in the electrostatic potential (ESP) is approximated using point charges (PC) as

$$v^K_{\mu\nu} \cong \tilde{v}^K_{\mu\nu} = \sum_{\mathrm{A}\in\mathrm{K}}\langle\mu|\frac{Q_\mathrm{A}}{|r-R_\mathrm{A}|}|\nu\rangle \tag{12}$$

where Q_A in eq 12 is the Mulliken population on atom A. The approximation is called the ESP-PC approximation[43] and is used in most FMO calculations.

The differentiation of the total FMO−DFT energy contains two components. One component contains terms from the internal fragment energies, E'_X; the second component contains terms from the ESP. The derivative of the internal fragment energy, E'_X, with respect to nuclear coordinate a, is

$$\frac{\partial E'_X}{\partial a} = \sum_{\mu\nu\in X} D^X_{\mu\nu}\frac{\partial h^X_{\mu\nu}}{\partial a} + \frac{1}{2}\sum_{\mu\nu\lambda\sigma\in X}\left[D^X_{\mu\nu}D^X_{\sigma\lambda} - \frac{c_x}{2}D^X_{\mu\lambda}D^X_{\nu\sigma}\right]\frac{\partial(\mu\nu|\lambda\sigma)}{\partial a} + \sum_{\mu\nu\in X} D^X_{\mu\nu}\int v^X_{xc}[\rho^X](\vec{r})\frac{\partial(\phi^X_\mu(\vec{r})\phi^X_\nu(\vec{r}))}{\partial a}\,\mathrm{d}\vec{r} + \sum_{\mu\nu\in X} D^X_{\mu\nu}\frac{\partial P^X_{\mu\nu}}{\partial a} - 2\sum_{i,j\in X}^{\mathrm{occ}} S^{a,X}_{ji}F'^X_{ji} - 4\sum_{i\in X}^{\mathrm{occ}}\sum_{r\in X}^{\mathrm{vir}} U^{a,X}_{ri}V^X_{ri} + \frac{\partial E^X_{NR}}{\partial a} + W^X_{xc} \tag{13}$$

dx.doi.org/10.1021/ct500808p | J. Chem. Theory Comput. 2014, 10, 5297−5307

The superscript a on S and U refer to a derivative with respect to coordinate a. The derivative of $E_{xc}^{X}[\rho^{X}]$, with respect to the nuclear coordinate a, is determined using eq 5 and the functional form of the chain rule.

$\nu_{xc}^{X}[\rho^{X}](\vec{r})$ is the exchange-correlation potential, $(\delta E_{xc}^{X}[\rho^{X}]/\delta\rho^{X}(\vec{r}))$, which is a functional of the density. Most exchange-correlation functionals are computed on a grid. In eq 13, W_{xc}^{X} arises from the derivative of the grid weights of $E_{xc}^{X}[\rho^{X}]$.[44] The reader is referred to ref 44 for more details about the derivative of grid weights. The internal fragment Fock matrix element is

$$F_{ij}^{\prime X} = h_{ij}^{X} + \sum_{k\in X}^{\mathrm{occ}} [2(ij|kk) - c_x(ik|jk)] + (i|v_{xc}^{X}|j) + P_{ij}^{X} \tag{14}$$

The term $(i|v_{xc}^{X}|j)$ is a matrix element of the exchange-correlation potential:

$$(i|v_{xc}^{X}|j) = \sum_{\mu,\nu\in X} C_{\mu i}^{X*} C_{\nu j}^{X} \int \phi_{\mu}^{X*}(\vec{r}) v_{xc}^{X}(\vec{r}) \phi_{\nu}^{X}(\vec{r})\, \mathrm{d}\vec{r} \tag{15}$$

P_{ij}^{X} is a matrix element of the HOP matrix

$$P_{ij}^{X} = \sum_{\mu\nu\in X} C_{\mu i}^{X*} P_{\mu\nu}^{X} C_{\nu j}^{X} \tag{16}$$

and the overlap derivative matrix $S_{ij}^{a,X}$ is

$$S_{ij}^{a,X} = \sum_{\mu\nu\in X} C_{\mu i}^{X*} \frac{\partial S_{\mu\nu}^{X}}{\partial a} C_{\nu j}^{X} \tag{17}$$

The term $S_{ji}^{a,X} F_{ji}^{\prime X}$ in eq 13 arises from the derivatives of the density matrix in eq 3, with respect to a nuclear coordinate. The orthonormality condition[31]

$$S_{ij}^{a,X} + U_{ji}^{a,X} + U_{ij}^{a,X} = 0 \tag{18}$$

was used to derive the $S_{ji}^{a,X} F_{ji}^{\prime X}$ term.

The following definition will be used for the response term $U_{ri}^{a,X}$:

$$\bar{U}^{a,X,Y} = 4 \sum_{i\in X}^{\mathrm{occ}} \sum_{r\in X}^{\mathrm{vir}} U_{ri}^{a,X} V_{ri}^{Y} \tag{19}$$

The response term arises from the derivative of the molecular orbital coefficient:

$$\frac{\partial C_{\mu i}^{X}}{\partial a} = \sum_{m\in X}^{\mathrm{occ+vir}} U_{mi}^{a,X} C_{\mu m}^{X} \tag{20}$$

$U_{ri}^{a,X}$ is determined by solving the CPKS equations.

Differentiation of the ESP term, with respect to nuclear coordinate a, is given as

$$\begin{aligned}\frac{\partial}{\partial a}\mathrm{Tr}(\Delta\mathbf{D}^{IJ}\mathbf{V}^{IJ}) = {} & \sum_{\mu\nu\in IJ} \Delta D_{\mu\nu}^{IJ} \sum_{\mathrm{K}\neq IJ}^{\mathrm{all}} \left[\frac{\partial u_{\mu\nu}^{\mathrm{K}}}{\partial a} + \sum_{\lambda\sigma\in \mathrm{K}} D_{\lambda\sigma}^{\mathrm{K}} \frac{\partial(\mu\nu|\lambda\sigma)}{\partial a} \right] \\ & - 2 \sum_{\mu\nu\in IJ} W_{\mu\nu}^{IJ} \frac{\partial S_{\mu\nu}^{I}}{\partial a} + 2 \sum_{\mu\nu\in I} W_{\mu\nu}^{I} \frac{\partial S_{\mu\nu}^{I}}{\partial a} \\ & + 2 \sum_{\mu\nu\in J} W_{\mu\nu}^{J} \frac{\partial S_{\mu\nu}^{J}}{\partial a} + \bar{U}^{a,IJ,IJ} - \bar{U}^{a,I,IJ} - \bar{U}^{a,J,IJ} \\ & - 2 \sum_{K\neq IJ}^{\mathrm{all}} \sum_{\mu\nu\in \mathrm{K}} \Delta X_{\mu\nu}^{\mathrm{K(IJ)}} S_{\mu\nu}^{a,\mathrm{K}} \\ & + 4 \sum_{\mathrm{K}\neq IJ}^{\mathrm{all}} \sum_{\mu\nu\in IJ} \sum_{r\in K}^{\mathrm{vir}} \sum_{i\in K}^{\mathrm{occ}} \Delta D_{\mu\nu}^{IJ} U_{ri}^{a,\mathrm{K}} (\mu\nu|ri)\end{aligned} \tag{21}$$

where

$$W_{\mu\nu}^{X} = \frac{1}{4} \sum_{\lambda\sigma\in X} D_{\mu\lambda}^{X} V_{\lambda\sigma}^{IJ} D_{\sigma\nu}^{X} \tag{22}$$

and

$$\Delta X_{\mu\nu}^{K(IJ)} = \frac{1}{4} \sum_{\lambda\sigma\in \mathrm{K}} D_{\mu\lambda}^{\mathrm{K}} [\sum_{\zeta\eta\in IJ} \Delta D_{\zeta\eta}^{IJ} (\zeta\eta|\lambda\sigma)] D_{\sigma\nu}^{\mathrm{K}} \tag{23}$$

Collecting all of the terms $\bar{U}^{a,X,Y}$ from eqs 13 and 21 forms the equation

$$\begin{aligned}\bar{U}^{a} = {} & -\sum_{I}^{N} \bar{U}^{a,I,I} - \sum_{I>J}^{N} (\bar{U}^{a,IJ,IJ} - \bar{U}^{a,I,I} - \bar{U}^{a,J,J}) \\ & + \sum_{I>J}^{N} (\bar{U}^{a,IJ,IJ} - \bar{U}^{a,I,IJ} - \bar{U}^{a,J,IJ})\end{aligned} \tag{24}$$

$\bar{U}^{a}$ is equal to zero when either no approximations are applied to the calculation of the ESP or approximations to the calculation of the ESP are applied uniformly. For most FMO calculations, the calculation of the ESP is approximated, but not uniformly; therefore, the contribution from $\bar{U}^{a}$ must be included in the gradient. The contribution from $\bar{U}^{a}$ has previously been included for the FMO-RHF method.[36] Since $\bar{U}^{a}$ only contains terms involving $\bar{U}_{ri}^{a,X}$ and V_{ri}^{Y}, the contributions to the gradient from $\bar{U}^{a}$ are identical for the FMO−RHF and FMO−DFT methods (the interested reader is referred to the previous study in refs 25 and 36). For the purposes of the derivation in the present study, $\bar{U}^{a}$ will be treated as being equal to zero; therefore, the only contributions to the gradient from $\bar{U}_{ri}^{a,\mathrm{K}}$ arise from the last term of eq 21. To find the last term of eq 21, it is necessary to solve the CPKS equations.

3. COUPLED PERTURBED KOHN−SHAM (CPKS) EQUATIONS FOR FMO−DFT

The FMO−DFT analytic gradient only contains response term contributions from monomers. The response term contributions can be found by exploiting the diagonal nature of the Fock matrix to solve the CPKS equations[41] for the FMO−DFT method.

For monomer I, the MO Fock matrix can be written as

$$\begin{aligned}F_{ij}^{I} &= F_{ij}^{\prime I} + V_{ij}^{I} \\ &= \tilde{h}_{ij}^{I} + \sum_{k\in I}^{\mathrm{occ}} [2(ij|kk) - c_x(ik|jk)] + (i|v_{xc}^{X}|j) + P_{ij}^{I}\end{aligned} \tag{25}$$

The FMO one-electron Hamiltonian is defined as

$$\tilde{h}_{ij}^{I} = h_{ij}^{I} + V_{ij}^{I} \tag{26}$$

The derivative of the monomer Fock matrix, with respect to a nuclear coordinate a, is defined as

$$\frac{\partial F_{ij}^{I}}{\partial a} = \frac{\partial}{\partial a}(\tilde{h}_{ij}^{I} + \sum_{k\in I}^{\mathrm{occ}} [2(ij|kk) - c_x(ik|jk)] + (i|v_{xc}^{X}|j) + P_{ij}^{I}) \tag{27}$$

Taking the derivative of the right side and rearranging terms, the derivative of the monomer Fock matrix, with respect to

dx.doi.org/10.1021/ct500808p | J. Chem. Theory Comput. 2014, 10, 5297−5307

nuclear coordinate a, can be written as

$$\frac{\partial F_{ij}^{I}}{\partial a} = F_{ij}^{a,I} + \sum_{k\in \mathrm{I}}^{\mathrm{occ+vir}} (U_{ki}^{a,I}F_{kj}^{I} + U_{kj}^{a,I}F_{ik}^{I}) + \sum_{k\in I}^{\mathrm{occ+vir}} \sum_{l\in \mathrm{I}}^{\mathrm{occ}} U_{kl}^{a,I}A'_{ij,kl} + \sum_{K\neq I} \sum_{k\in \mathrm{K}}^{occ+vir} \sum_{l\in \mathrm{K}}^{occ} U_{kl}^{a,\mathrm{K}} 4(ij|kl) \tag{28}$$

The orbital Hessian matrix A' is defined as

$$A'_{ij,kl} = 4(ij|kl) - c_x[(ik|jl) + (il|jk)] + 4(ij|f_{xc}^{X}|kl) \tag{29}$$

The term $(ij|f_{xc}^{X}|kl)$ is the matrix element of the exchange-correlation kernel:

$$f_{xc}^{X}[\rho^{X}](\vec{r}, \vec{r}') = \frac{\delta^2 E_{xc}^{X}[\rho^{X}]}{\delta\rho^{X}(\vec{r})\delta\rho^{X}(\vec{r}')} \tag{30}$$

$$(ij|f_{xc}^{X}|kl) = \sum_{\mu,\nu,\rho,\sigma\in X} C_{\mu i}^{X*} C_{\nu j}^{X} C_{\rho k}^{X*} C_{\sigma l}^{X} \times \iint \phi_{\mu}^{X*}(\vec{r})\phi_{\nu}^{X}(\vec{r}) f_{xc}^{X}(\vec{r}, \vec{r}')\phi_{\rho}^{X*}(\vec{r}')\phi_{\sigma}^{X}(\vec{r}')\, \mathrm{d}\vec{r}\, \mathrm{d}\vec{r}' \tag{31}$$

The derivative of the Fock matrix element is

$$F_{ij}^{a,I} = h_{ij}^{a,I} + V_{ij}^{a,I} + \sum_{k\in \mathrm{I}}^{\mathrm{occ}} [2(ij|kk)^{a} - c_x(ik|jk)^{a}] + (i|v_{xc}^{X}|j)^{a} + P_{ij}^{a,I} \tag{32}$$

$h_{ij}^{a,I}$ is the derivative of the one-electron Hamiltonian,

$$h_{ij}^{a,I} = \sum_{\mu\nu\in I} C_{\mu i}^{I*} C_{\nu j}^{I} \frac{\partial h_{\mu\nu}^{I}}{\partial a} \tag{33}$$

The derivative of the two-electron integral $(ij|kl)^{a}$ is

$$(ij|kl)^{a} = \sum_{\mu\nu\rho\sigma} C_{\mu i}^{I*} C_{\nu j}^{I} C_{\rho k}^{I*} C_{\sigma l}^{I} \frac{\partial(\mu\nu|\rho\sigma)}{\partial a} \tag{34}$$

and the derivative of the exchange-correlation potential matrix elements $(i|v_{xc}^{X}|j)^{a}$ is

$$(i|v_{xc}^{X}|j)^{a} = \sum_{\mu,\nu\in X} C_{\mu i}^{X*} C_{\nu j}^{X} \int v_{xc}^{X}(\vec{r}) \frac{\partial(\phi_{\mu}^{X*}(\vec{r})\phi_{\nu}^{X}(\vec{r}))}{\partial a}\, \mathrm{d}\vec{r} + 2 \sum_{\mu,\nu,\rho,\sigma\in X} \sum_{k\in X}^{\mathrm{occ}} C_{\mu i}^{X*} C_{\nu j}^{X} C_{\rho k}^{X*} C_{\sigma k}^{X} \times \iint \phi_{\mu}^{X*}(\vec{r})\phi_{\nu}^{X}(\vec{r}) f_{xc}^{X}(\vec{r}, \vec{r}') \frac{\partial(\phi_{\rho}^{X*}(\vec{r}')\phi_{\sigma}^{X}(\vec{r}'))}{\partial a}\, \mathrm{d}\vec{r}\, \mathrm{d}\vec{r}' \tag{35}$$

The functional form of the chain rule and the relationship

$$\frac{\delta v_{xc}^{X}[\rho^{X}](\vec{r})}{\delta\rho^{X}(\vec{r}')} = \frac{\delta^2 E_{xc}^{X}[\rho^{X}]}{\delta\rho^{X}(\vec{r})\delta\rho^{X}(\vec{r}')} = f_{xc}^{X}[\rho^{X}](\vec{r}, \vec{r}') \tag{36}$$

is used to derive $(i|v_{xc}^{X}|j)^{a}$.

The ESP derivative $V_{ij}^{a,I}$ is defined as

$$V_{ij}^{a,I} = \sum_{K\notin I} (u_{ij}^{a,K} + \sum_{k\in \mathrm{K}}^{\mathrm{occ}} 2(ij|kk)^{a}) \tag{37}$$

The one-electron derivative contribution, $u_{ij}^{a,K}$, in eq 37 and the HOP derivative $P_{ij}^{a,I}$ in eq 32 are defined in an analogous manner to the derivative of the one-electron Hamiltonian $h_{ij}^{a,I}$ in eq 33.

Further rearrangement of eq 28 leads to

$$\frac{\partial F_{ij}^{I}}{\partial a} = F_{ij}^{a,I} - (\varepsilon_{j}^{I} - \varepsilon_{i}^{I})U_{ij}^{a,I} - S_{ij}^{a,I}\varepsilon_{j}^{I} - \sum_{k,l\in I}^{\mathrm{occ}} S_{kl}^{a,I}[2(ij|kl) - c_x(ik|jl)] + \sum_{k\in \mathrm{I}}^{\mathrm{vir}} \sum_{l\in \mathrm{I}}^{\mathrm{occ}} U^{a,I}A'_{ij,kl} - \sum_{K\neq I} \sum_{k,l\in \mathrm{K}}^{\mathrm{occ}} 2S_{kl}^{a,\mathrm{K}}(ij|kl) + \sum_{\mathrm{K}\neq I} \sum_{k\in \mathrm{K}}^{\mathrm{vir}} \sum_{l\in \mathrm{K}}^{\mathrm{occ}} U_{kl}^{a,\mathrm{K}} 4(ij|kl) \tag{38}$$

where ε_{i}^{I} is the energy of MO i of fragment I. The orthonormality condition[16] of eq 18 was used to derive eq 38.

For each fragment I, eq 38 contains $U_{kl}^{a,X}$ contributions from all fragments in the system. Therefore, the $\partial F_{ij}^{X}/\partial a$ for each fragment are coupled and must be collected and solved together. The $\partial F_{ij}^{X}/\partial a$ for all fragments can be written in matrix form as

$$\mathbf{A}\mathbf{U}^{a} = \mathbf{B}_{0}^{a} \tag{39}$$

The fragment block diagonal part of matrix $\mathbf{A}$ is

$$A_{ij,kl}^{I,I} = \delta_{ik}\delta_{jl}(\varepsilon_{j}^{I} - \varepsilon_{i}^{I}) - \{4(ij|kl) - c_x[(ik|jl) + (il|jk)] + 4(ij|f_{xc}^{X}|kl)\} \tag{40}$$

the fragment off-diagonal part is

$$A_{ij,kl}^{I,K} = -4(ij|kl) \tag{41}$$

and the ijth element of the vector $\mathbf{B}_{0}^{a}$ for fragment I is

$$B_{0,ij}^{a,I} = F_{ij}^{a,I} - S_{ij}^{a,I}\varepsilon_{j}^{I} - \sum_{kl\in \mathrm{I}}^{\mathrm{occ}} S_{kl}^{a,\mathrm{I}}[2(ij|kl) - c_x(ik|jl)] - \sum_{\mathrm{K}\neq I} \sum_{kl\in \mathrm{K}}^{\mathrm{occ}} 2S_{kl}^{a,\mathrm{K}}(ij|kl) \tag{42}$$

The response terms for the FMO−DFT gradient can be included by applying the SCZV procedure to eq 39 in a manner identical to the FMO−RHF gradient. Of course, the definitions of matrix $\mathbf{A}$ and vector $\mathbf{B}_{0}^{a}$ are different for FMO−DFT. (Readers interested in the SCZV procedure for the FMO−DFT method are directed to the previous study of the analytic gradient for the FMO-RHF method.[25])

The analytic FMO−DFT gradient was implemented in GAMESS[45] and parallelized with the generalized distributed data interface.[46]

4. COMPUTATIONAL DETAILS

To demonstrate that the inclusion of the response terms makes the FMO−DFT gradient fully analytic, gradient calculations with and without the response terms included were compared to numerical gradients. For comparison purposes, the error in the numerical gradient is set to zero. To test the accuracy of the gradient for systems with and without fragmentation across a covalent bond, two test systems were chosen: a $(H_2O)_{32}$ cluster (Figure 1a) and an alanine $(ALA)_7$ polypeptide chain in an α helix configuration (Figure 1b). For both test systems, calculations were performed with several density functionals. A distance cutoff of 2.0 (unitless) was used for the ESP-PTC approximation (RESPPC) and the electrostatic dimer approximation (RESDIM) for all calculations. For the RESPPC and RESDIM cutoffs, the distance between two atoms A and B is

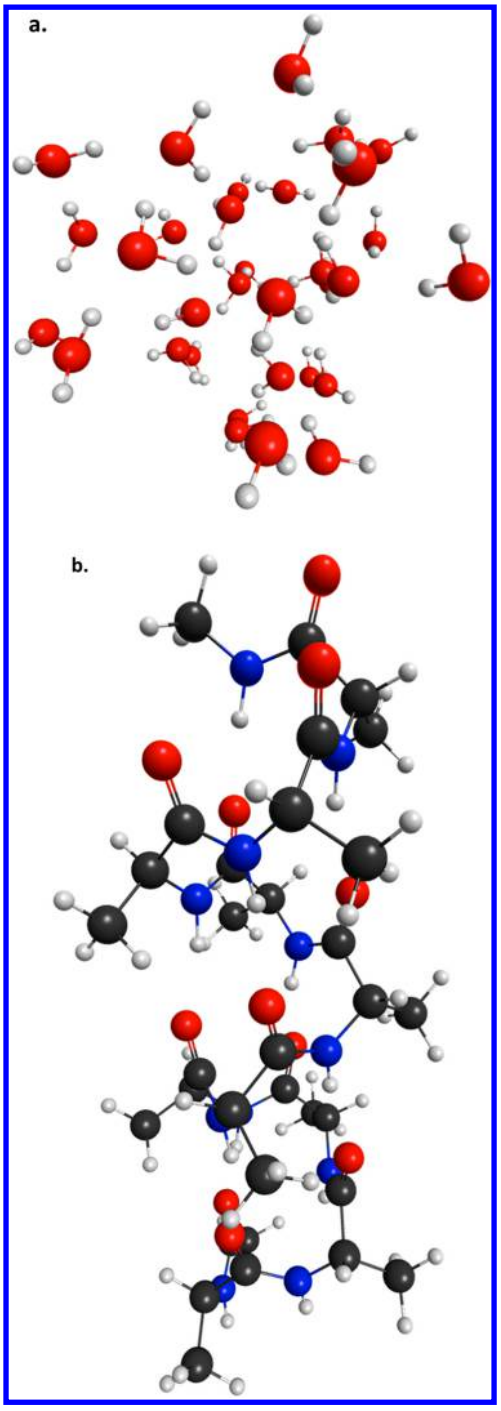

Figure 1. Geometric structures of (a) $(H_2O)_{32}$, (b) $(Ala)_7$ [colored by chemical elements as black (C), red (O), blue (N), and gray (H)].

defined relative to the van der Waals radii of atoms A and B, $R_{AB}/(R_A + R_B)$, where R_{AB} is the Euclidean distance between atoms A and B and R_A is the van der Waals radius of atom A. For the gradient calculations with response terms, $\bar{U}^a$ from eq 24 was included in the gradient.[25,36] The numerical energy gradient was calculated using double differencing with a step size of 0.0001 and 0.0005 Å for the $(H_2O)_{32}$ cluster and the $(ALA)_7$ polypeptide chain, respectively.

For the 32-water cluster, an additional calculation was performed without the ESP-PTC approximation or the electrostatic dimer approximation (a cutoff of 0.0) to quantify how much error is introduced into the gradient calculation through the use of the two approximations. For the water cluster, each water molecule was treated as a fragment, while for the alanine polypeptide chain, each alanine unit was treated as a fragment.

Table 1. Maximum Absolute Gradient Value (MAX), the Root Mean Square of the Errors (RMS Error), and the Maximum Absolute Error in Any Gradient Element (MAX Error) for the FMO Gradient with and without Response Terms Included for the $(H_2O)_{32}$ Cluster[a]

gradient	MAX	RMS error	MAX error
$(H_2O)_{32}$, B3LYP/6-31G(d), RESPPC = 2.0, RESDIM = 2.0			
with response terms	0.031425	0.000023	0.000100
without response terms	0.029790	0.000613	0.002122
$(H_2O)_{32}$, PBE0/6-31G(d), RESPPC = 2.0, RESDIM = 2.0			
with response terms	0.029265	0.000019	0.000071
without response terms	0.029586	0.000377	0.001567
$(H_2O)_{32}$, BLYP/6-31G(d), RESPPC = 2.0, RESDIM = 2.0			
with response terms	0.040782	0.000032	0.000132
without response terms	0.040278	0.000451	0.001649
$(H_2O)_{32}$, SVWN/6-31G(d), RESPPC = 2.0, RESDIM = 2.0			
with response terms	0.048558	0.000016	0.000057
without response terms	0.049120	0.000421	0.001561
$(H_2O)_{32}$, B3LYP/6-31G(d), RESPPC = 0.0, RESDIM = 0.0			
with response terms	0.031230	0.000017	0.000053
without response terms	0.031218	0.000164	0.000747
$(H_2O)_{32}$, B3LYP/6-311G(2d,2p), RESPPC = 2.0, RESDIM = 2.0			
with response terms	0.024845	0.000033	0.000125
without response terms	0.024612	0.000612	0.0003325
$(H_2O)_{32}$, HF/6-31G(d), RESPPC = 2.0, RESDIM = 2.0			
with response terms	0.029817	0.000014	0.000043
without response terms	0.029600	0.000327	0.001520

[a]The error in the numerical gradients is set to zero. Atomic units are used.

Additional DFT calculations in which no fragmentation was used were performed on the water cluster systems to check the accuracy of the FMO−DFT gradient relative to fully *ab initio* methods. For the additional calculations, the B3LYP, PBE0, and SVWN functionals were used. All the DFT calculations were performed using the 6-31G(d) basis.

To demonstrate that the inclusion of the response terms in the FMO−DFT gradient results in improved energy conservation in the NVE ensemble, MD calculations with and without the response terms included in the FMO−DFT gradient were performed on a system of 12 dichloromethane molecules. The FMO−DFT MD calculations were performed for 3 ps using a range of step sizes from 0.33 fs to 1.25 fs. For all MD simulations, the B3LYP functional and the 6-31G basis set were used. The initial geometry of the dichloromethane cluster was obtained by optimizing a random initial cluster of 12 dichloromethane molecules using FMO−DFT with the B3LYP functional and the 6-31G basis set. The initial velocities of the dichloromethane cluster were randomly initialized so that the temperature of the system was 300 K. All MD simulations used the same initial velocities. Similar to previous FMO MD calculations with the analytic energy gradient, a spherical solvent boundary potential was used to prevent evaporation.[29] In the present study, the force constant for the spherical boundary potential was set to 2.0 kcal/mol/Å^2 and the radius of the sphere was set to 4.5 Å. All FMO−DFT MD simulations used a value of 2.0 for the ESP-PC and ES-DIM approximations. The velocity−Verlet algorithm was used to integrate the equations of motion.

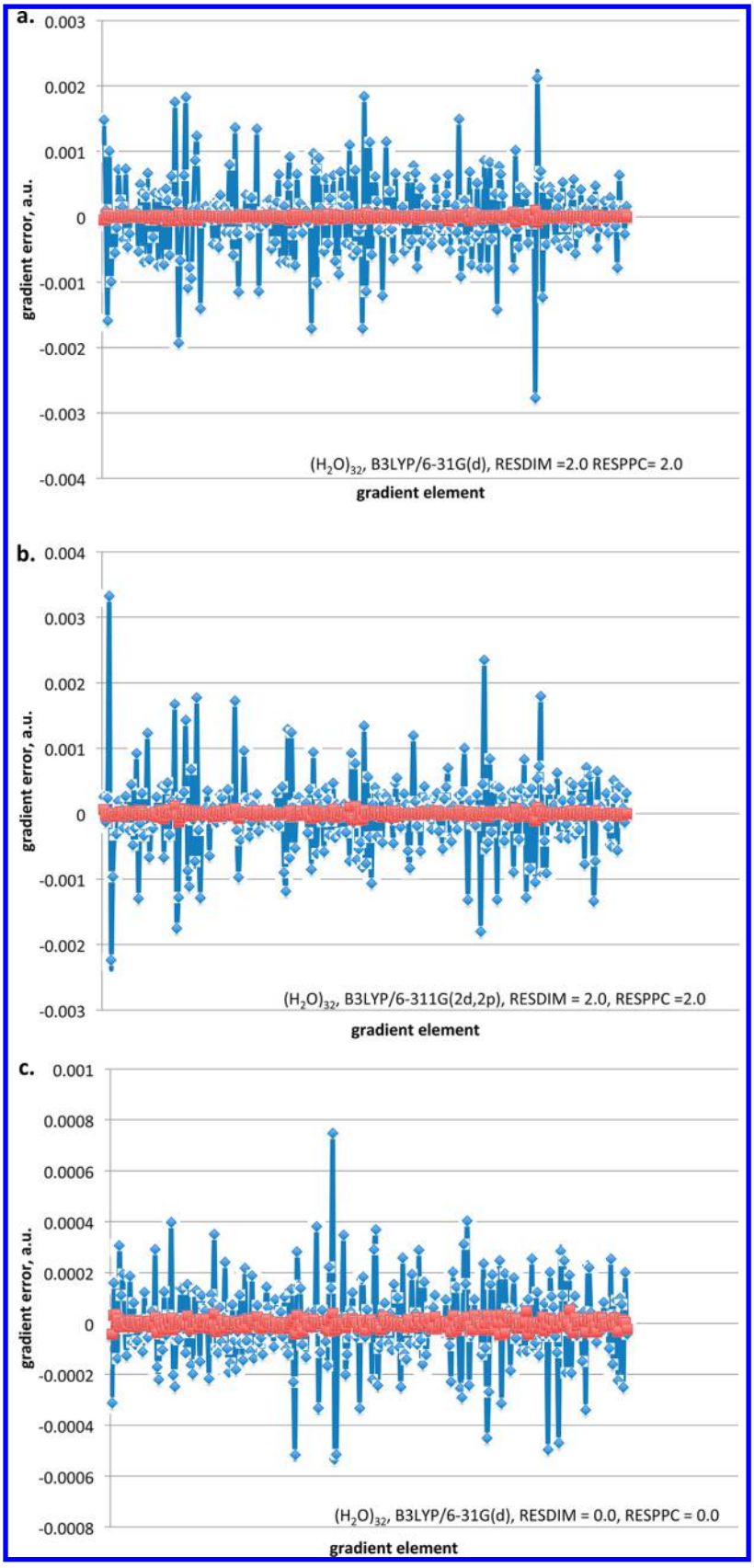

Figure 2. Error of each gradient element relative to the numeric gradient for the $(H_2O)_{32}$ test system for (a) B3LYP/6-31G(d), RESDIM = 2.0, RESPPC = 2.0; (b) B3LYP/6-311G(2d,2p), RESDIM = 2.0, RESPPC = 2.0; and (c) B3LYP/6-31G(d), RESDIM = 0.0, RESPPC = 0.0. Red squares are the gradient with response terms included in the gradient; blue squares are the gradient without response terms included in the gradient.

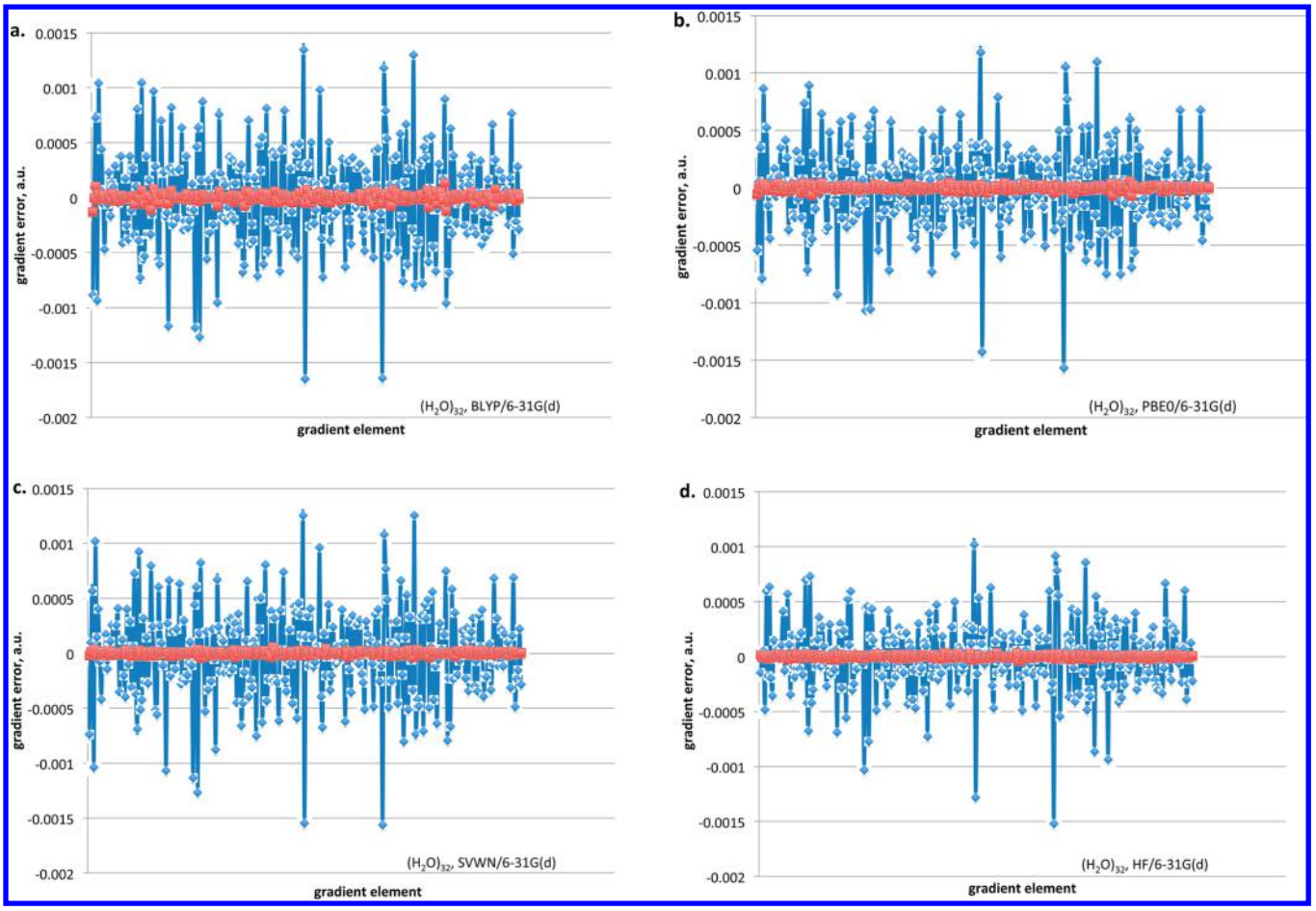

Figure 3. Error of each gradient element relative to the numeric gradient for the $(H_2O)_{32}$ test system for (a) BLYP/6-31G(d), (b) PBE0/6-31G(d), (c) SVWN/6-31G(d), and (d) HF/6-31G(d). Red squares are the gradient with response terms included in the gradient; blue squares are the gradient without response terms included in the gradient. RESDIM and RESPPC were set to 2.0 for all calculations.

Table 2. Maximum Absolute Gradient Value (MAX), the Root Mean Square of the Errors (RMS Error), and the Maximum Absolute Error in Any Gradient Element (MAX Error) for the FMO Gradient with and without Response Terms Included for the $(ALA)_7$ Polypeptide[a]

gradient	MAX	RMS error	MAX error
$(ALA)_7$, B3LYP/6-31G(d)			
with response terms	0.631294	0.000010	0.000038
without response terms	0.631309	0.000332	0.001308
$(ALA)_7$, PBE0/6-31G(d)			
with response terms	0.635749	0.0000091	0.000018
without response terms	0.635756	0.000336	0.001279
$(ALA)_7$, HF/6-31G(d)			
with response terms	0.635648	0.0000098	0.000054
without response terms	0.635691	0.000285	0.001349

[a]RESDIM and RESPPC were set to 2.0 for all calculations. The error in the numerical gradients is set to zero. Atomic units are used.

For each FMO MD simulation, the root-mean-square deviation (RMSD) of the energy was calculated. In the velocity–Verlet algorithm, the RMSD of the energy is proportional to the square of the time step. Therefore, a double-logarithmic graph of the RMSD of the energy versus the time step should be linear with a slope of 2.0. Ideally, a DFT-MD simulation without fragmentation (no FMO) should be performed to compare with the FMO–DFT MD simulations. Unfortunately, because of the high computational cost, DFT MD is not computationally feasible for the system presented here. However, previous studies[28,29] have shown that FMO MD consistently produces a larger energy RMSD than an MD calculation without fragmentation. Therefore, in a previous study,[30] the assumption was made that, when comparing two FMO-MD calculations with different gradients, a lower RMSD of the energy represents a more-accurate value for a given time step. The assumption also is adopted in the present study.

All FMO–DFT and DFT calculations in this study used a grid to evaluate the exchange-correlation functional. The grid contained 96 radial points for the Euler–MacLaurin quadrature and 302 angular points for the Lebedev grid.

5. RESULTS AND DISCUSSION

Results from the gradient calculations for the water test system are presented in Table 1. For all functionals, inclusion of the response terms results in a more-accurate gradient. For the water system, the error in each gradient element with and without response terms is presented in Figure 2 for calculations using the B3LYP functional and Figure 3 for calculations using all non-B3LYP functionals, and Hartree–Fock. For the four water cluster systems for which calculations were performed with the 6-31G(d) basis and the ESP-PTC and electrostatic dimer approximations, the root-mean-square (RMS) error improves with the inclusion of response terms by a minimum factor of 13 to a maximum factor of 26.

dx.doi.org/10.1021/ct500808p | J. Chem. Theory Comput. 2014, 10, 5297–5307

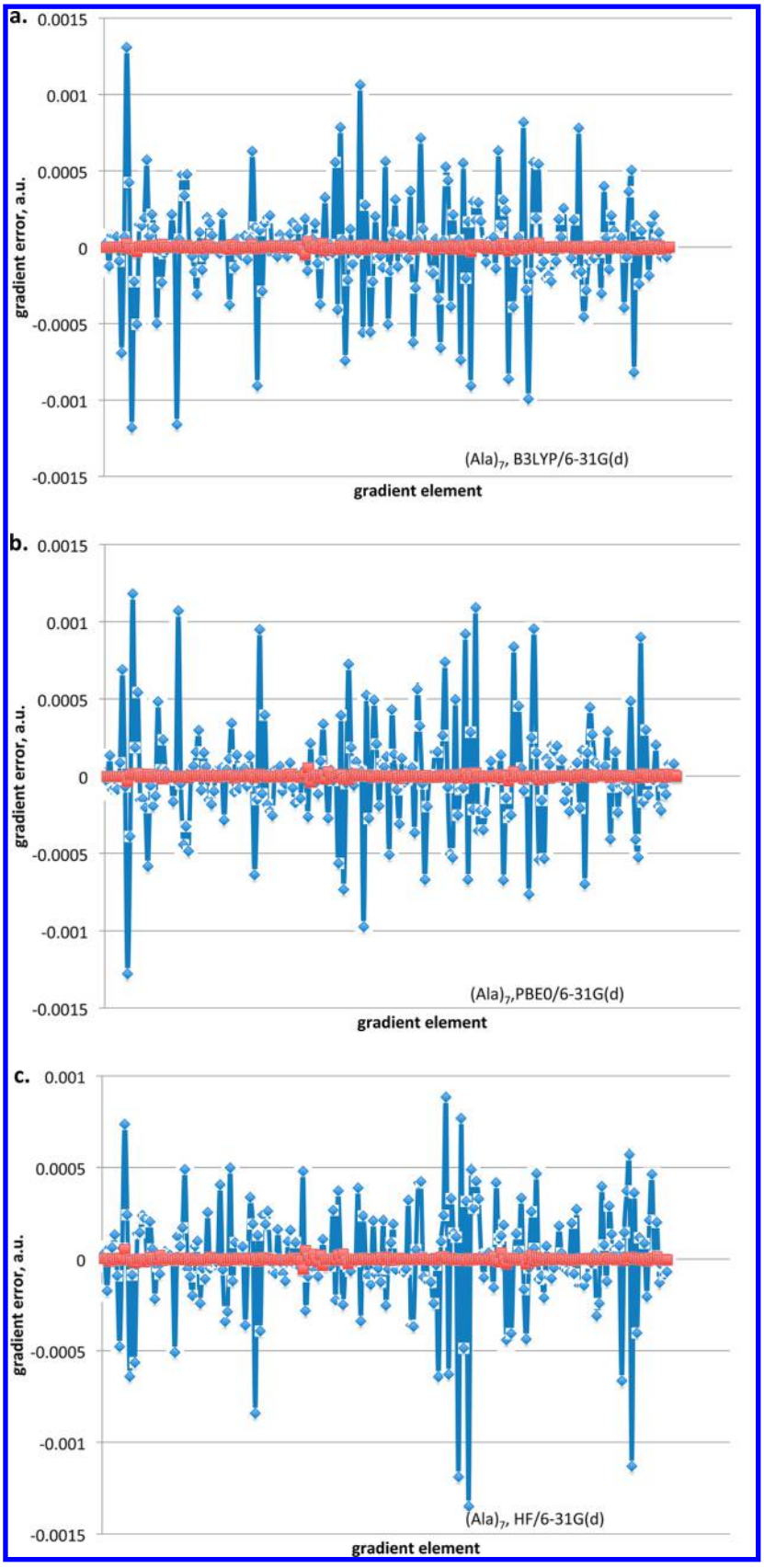

Figure 4. Error of each gradient element relative to the numeric gradient for the $(Ala)_7$ test system for (a) B3LYP/6-31G(d), (b) PBE0/6-31(d), and (c) HF/6-31G(d). Red squares are the gradient with response terms included in the gradient; blue squares are the gradient without response terms included in the gradient. RESDIM and RESPPC were set to 2.0 for all calculations.

Table 3. Comparison of the FMO−DFT and DFT Gradients for the $(H_2O)_{32}$ Cluster with Response Terms Included[a]

MAX[b]	RMSD[c]	MAX diff[d]
	$(H_2O)_{32}$, B3LYP/6-31G(d)	
0.031425	0.001349	0.00544
	$(H_2O)_{32}$, PBE0/6-31G(d)	
0.029265	0.001176	0.00426
	$(H_2O)_{32}$, SVWN/6-31G(d)	
0.048558	0.001558	0.00533

[a]RESDIM and RESPPC were set to 2.0 for all FMO calculations. Atomic units are used. [b]MAX = the maximum absolute value in the FMO−DFT gradient. [c]RMSD = the root mean square difference between FMO−DFT gradient elements and DFT gradient elements. [d]MAX diff = the maximum absolute difference between a FMO−DFT gradient element and a DFT gradient element.

There is a negligible increase in the gradient error when the ESP-PTC and electrostatic dimer approximations are used for the B3LYP water cluster. Specifically, the RMS error increases from 0.000017 hartree/bohr to 0.000023 hartree/bohr when the approximations are included in the calculation. Although the negligible increase in error indicates that the ESP-PTC and electrostatic dimer approximations can be reliably applied in FMO−DFT gradient calculations, care must be taken when using the ESP-PTC approximation. A previous study[36] using the FMO-RHF method has determined that the van der Waals (vdw) radius cutoff for the ESP-PTC approximation should be set above 2.0 for accurate calculations. To assess the effect of the basis set, a test calculation was performed with the 6-311G(2d,2p) basis for the water cluster system with the B3LYP functional. Inclusion of the response terms reduces the RMS error for the system by more than a factor of 18. The factor is similar in magnitude to that obtained from calculations that use the 6-31G(d) basis set, indicating that the inclusion of the response terms gives an accurate gradient for any basis set.

An additional calculation was performed on the water cluster using the FMO−RHF method (see Figure 3d) to compare the accuracy of the FMO−DFT gradient to the FMO−RHF gradient. For the FMO−RHF gradient, the inclusion of the response terms reduces the RMS error by a factor of 23. The reduction in the RMS error for the FMO-RHF gradient is similar in magnitude to the reduction in the RMS error for the FMO−DFT gradient when response terms are included, and it indicates that the analytic gradient for FMO−DFT is as accurate as that for the FMO−RHF method.

Results from the gradient calculation on the alanine peptide system are presented in Table 2. Similar to the water system, inclusion of the response terms results in a more-accurate gradient for all test systems. For the alanine peptide system, the errors in each gradient element with and without the response terms included are presented in Figure 4. The RMS error improves by a factor of 34 for the B3LYP functional and by a factor of 36 for the PBE0 functional. A previous study[25] found that the FMO−RHF gradient is accurate for a system of bonded fragments. Therefore, a calculation at the FMO−RHF/6-31G(d) level of theory was performed on the alanine peptide system. Inclusion of the response terms for the alanine peptide system at the FMO−RHF/6-31G(d) level of theory improves the RMS error by a factor of 29. Since the decrease in the RMS error for the FMO−RHF gradient is of the same order of magnitude as that for the FMO−DFT gradient, the FMO−DFT gradient is as accurate as the FMO−RHF gradient for systems with either bonded or nonbonded fragments.

Since the SCZV procedure for FMO−DFT is similar for different functionals, the error in the gradient due to the SCZV procedure should be of similar magnitude for different functionals. This is demonstrated in the present study, since the FMO−DFT gradient is not significantly more accurate for any test functional. Therefore, the FMO−DFT gradient derived and implemented here can be applied to any functional.

Comparison of the FMO−DFT gradient with the DFT gradient with no fragmentation of the system is presented in Table 3. For all three functionals, the FMO−DFT gradient reproduces the DFT gradient. Of the three test functionals, the maximum RMS deviation of the FMO−DFT gradient from the DFT gradient is 0.0016 hartree/bohr with the SVWN functional. For the three test functionals, the largest difference

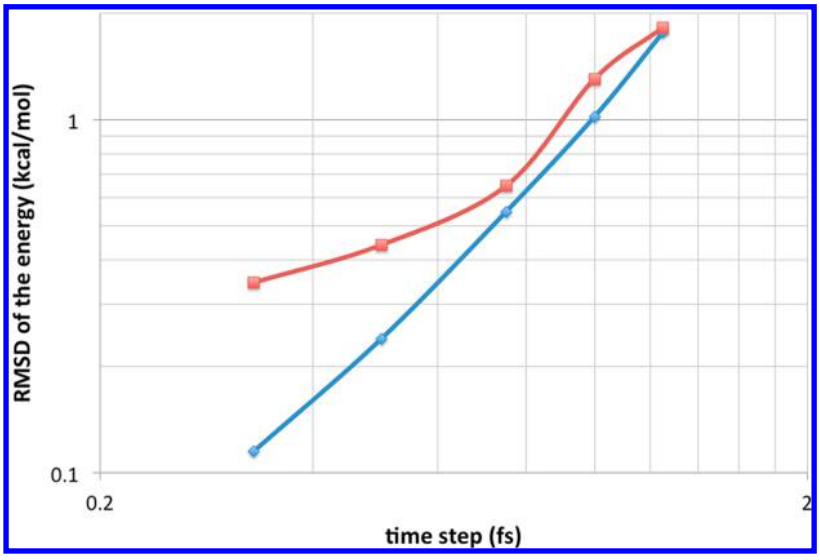

Figure 5. Double logarithmic plots of the energy RMSD versus the time step for the FMO MD simulations on a cluster of 12 dichloromethane molecules. Data for FMO MD calculations with response terms included in the gradient are shown in blue; data for FMO-MD calculations without response terms included in the gradient are shown in red.

dx.doi.org/10.1021/ct500808p | J. Chem. Theory Comput. 2014, 10, 5297−5307

in any single gradient element is 0.00554 hartree/bohr and occurs when the B3LYP functional is used.

The double logarithmic plot of the RMSD of the energy versus the time step for the FMO MD simulations of 12 dichloromethane molecules with and without response terms included in the gradient is presented in Figure 5. The FMO−DFT MD simulations, with response terms included in the gradient, show an almost linear relationship with a slope of 2.07 for the linear line of best fit near the theoretical value of 2.0 for the velocity-Verlet algorithm. The close agreement of the calculated slope with the theoretical value indicates that FMO−DFT MD with response terms included in the gradient results in energy conservation in the NVE ensemble. The line of best fit for the FMO−DFT MD simulations without response terms included in the gradient is not linear and, instead, branches upward, indicating worse energy conservation than that for the FMO−DFT MD simulations in which response terms are included in the energy gradient. The energy RMSD values for all of the MD simulations are collected in Table 4. When the response terms are included, the energy RMSD is lower for each time step in the FMO−DFT MD simulation, indicating that the FMO−DFT MD simulations with the response terms included give better energy conservation than FMO−DFT MD simulations without the response terms.

Table 4. RMSD of the Energy for the FMO MD Simulations on a Cluster of 12 Dichloromethane Molecules

	RMSD of the Energy (kcal/mol)	
time step (fs)	with response terms	without response terms
0.33	0.11	0.35
0.5	0.24	0.44
0.75	0.55	0.65
1.0	1.02	1.31
1.25	1.77	1.82

6. CONCLUSIONS

For *ab initio* methods, accurate gradients are a necessity for the calculation of properties, verification of potential energy minima, and molecular dynamics simulations. In the present study, the analytic gradient has been derived and the implementation has been discussed for the FMO2−DFT method, using the SCZV procedure previously derived for the FMO−RHF gradient. Inclusion of the response terms results in a more-accurate gradient when compared to numerical gradients for all test systems. Given the increased accuracy, the response terms should be included for all FMO−DFT MD calculations. The FMO−DFT gradient reproduces the DFT gradient in which no fragmentation has been performed, and it is a potential linearly scaling DFT method that can be combined with molecular dynamics. Response terms are now included in the FMO gradient for RHF, UHF, MP2, and DFT, and a future promising research direction will be to extend the analytic gradient to other FMO methods, such as multilayer FMO,[47] three-body FMO,[48] FMO with an auxiliary basis set,[49] and the effective fragment molecular orbital method.[50]

AUTHOR INFORMATION

Corresponding Author

*E-mails: mark@si.msg.chem.iastate.edu, gordon@ameslab.gov.

Notes

The authors declare no competing financial interest.

ACKNOWLEDGMENTS

K.R.B. was supported by a Department of Energy Computational Science Graduate Fellowship. F.Z. and M.S.G. were supported by funds provided by the Department of Energy, Basic Energy Sciences, to the Ames Laboratory, administered by Iowa State University. The Ames Laboratory is operated for the U.S. Department of Energy by Iowa State University, under Contract No. DE-AC02-07CH11358. D.G.F. was supported by the Next Generation Super Computing Project, Nanoscience Program (MEXT, Japan) and Computational Materials Science Initiative (CMSI, Japan). The computations reported here were performed on the Cyence computer at Iowa State University, obtained via a U.S. National Science Foundation MRI grant.

REFERENCES

(1) Kitaura, K.; Ikeo, E.; Asada, T.; Nakano, T.; Uebayasi, M. *Chem. Phys. Lett.* **1999**, *313*, 701−706.
(2) Gordon, M. S.; Fedorov, D. G.; Pruitt, S. R.; Slipchenko, L. V. *Chem. Rev.* **2012**, *112*, 632−672.
(3) Otto, P.; Ladik, J. *Chem. Phys.* **1975**, *8*, 192−200.
(4) Yang, W. *Phys. Rev. Lett.* **1991**, *66*, 1438.
(5) Gao, J. *J. Phys. Chem. B* **1997**, *101*, 657−663.
(6) Kobayashi, M.; Nakai, H. *Phys. Chem. Chem. Phys.* **2012**, *14*, 7629−7639.
(7) Aoki, Y.; Gu, F. L. *Phys. Chem. Chem. Phys.* **2012**, *14*, 7640−7668.
(8) Kurbanov, E. K.; Leverentz, H. R.; Truhlar, D. G.; Amin, E. A. *J. Chem. Theory Comput.* **2012**, *8*, 1−5.
(9) Yeole, S. D.; Gadre, S. R. *J. Chem. Phys.* **2010**, *132*, 094102.
(10) Jacob, C. R.; Visscher, L. *J. Chem. Phys.* **2008**, *128*, 155102.
(11) Hua, S.; Hua, W.; Li, S. *J. Phys. Chem. A* **2010**, *114*, 8126−8134.
(12) Goedecker, S.; Scuseria, G. E. *Comput. Sci. Eng.* **2003**, *5*, 14−21.
(13) Sawada, T.; Fedorov, D. G.; Kitaura, K. *J. Am. Chem. Soc.* **2010**, *132*, 16862−16872.
(14) Alexeev, Y.; P Mazanetz, M.; Ichihara, O.; Fedorov, D. G. *Curr. Top. Med. Chem.* **2012**, *12*, 2013−2033.
(15) Watanabe, T.; Inadomi, Y.; Fukuzawa, K.; Nakano, T.; Tanaka, S.; Nilsson, L.; Nagashima, U. *J. Phys. Chem. B* **2007**, *111*, 9621−9627.
(16) Carlson, P. J.; Bose, S.; Armstrong, D. W.; Hawkins, T.; Gordon, M. S.; Petrich, J. W. *J. Phys. Chem. B* **2011**, *116*, 503−512.
(17) Avramov, P. V.; Fedorov, D. G.; Sorokin, P. B.; Sakai, S.; Entani, S.; Ohtomo, M.; Naramoto, H. *J. Phys. Chem. Lett.* **2012**, *3*, 2003−2008.
(18) Sugiki, S. I.; Kurita, N.; Sengoku, Y.; Sekino, H. *Chem. Phys. Lett.* **2003**, *382*, 611−617.
(19) Fedorov, D. G.; Kitaura, K. *Chem. Phys. Lett.* **2004**, *389*, 129−134.
(20) Fedorov, D. G.; Kitaura, K. *J. Phys. Chem. A* **2007**, *111*, 6904−6914.
(21) Fedorov, D. G.; Nagata, T.; Kitaura, K. *Phys. Chem. Chem. Phys.* **2012**, *14*, 7562−7577.
(22) Tanaka, S.; Mochizuki, Y.; Komeiji, Y.; Okiyama, Y.; Fukuzaw, K. *Phys. Chem. Chem. Phys.* **2014**, *16*, 10310−10344.
(23) Fedorov, D. G., Kitaura, K., Eds. *The Fragment Molecular Orbital Method: Practical Applications to Large Molecular Systems*; CRC Press: Boca Raton, FL, 2009.
(24) Kitaura, K.; Sugiki, S. I.; Nakano, T.; Komeiji, Y.; Uebayasi, M. *Chem. Phys. Lett.* **2001**, *336*, 163−170.
(25) Nagata, T.; Brorsen, K.; Fedorov, D. G.; Kitaura, K.; Gordon, M. S. *J. Chem. Phys.* **2011**, *134*, 124115.
(26) Nagata, T.; Fedorov, D. G.; Kitaura, K. *Chem. Phys. Lett.* **2009**, *475*, 124−131.
(27) Nagata, T.; Fedorov, D. G.; Kitaura, K. *Chem. Phys. Lett.* **2010**, *492*, 302−308.
(28) Komeiji, Y.; Nakano, T.; Fukuzawa, K.; Ueno, Y.; Inadomi, Y.; Nemoto, T.; Kitaura, K. *Chem. Phys. Lett.* **2003**, *372*, 342−347.
(29) Komeiji, Y.; Mochizuki, Y.; Nakano, T.; Fedorov, D. G. *J. Mol. Struct. THEOCHEM* **2009**, *898*, 2−7.

(30) Brorsen, K. R.; Minezawa, N.; Xu, F.; Windus, T. L.; Gordon, M. S. *J. Chem. Theory Comput.* **2012**, *8*, 5008−5012.
(31) Yamaguchi, Y.; Schaefer, H. F., III; Osamura, Y.; Goddard, J. *A New Dimension to Quantum Chemistry: Analytical Derivative Methods in Ab Initio Molecular Electronic Structure Theory*; Oxford University Press: New York, 1994.
(32) Handy, N. C.; Schaefer, H. F., III. *J. Chem. Phys.* **1984**, *81*, 5031−5033.
(33) Ochsenfeld, C.; Head-Gordon, M. *Chem. Phys. Lett.* **1997**, *270*, 399−405.
(34) Nakata, H.; Fedorov, D. G.; Nagata, T.; Yokojima, S.; Ogata, K.; Kitaura, K.; Nakamura, S. *J. Chem. Phys.* **2012**, *137*, 044110.
(35) Nagata, T.; Fedorov, D. G.; Ishimura, K.; Kitaura, K. *J. Chem. Phys.* **2011**, *135*, 044110.
(36) Nagata, T.; Fedorov, D. G.; Kitaura, K. *Chem. Phys. Lett.* **2012**, *544*, 87−93.
(37) Nakata, H.; Fedorov, D. G.; Yokojima, S.; Kitaura, K.; Nakamura, S. *Theor. Chem. Acc.* **2014**, *133*, 1−14.
(38) Nagata, T.; Fedorov, D. G.; Li, H.; Kitaura, K. *J. Chem. Phys.* **2012**, *136*, 204112.
(39) Nagata, T.; Fedorov, D. G.; Kitaura, K. *Theor. Chem. Acc.* **2012**, *131*, 1−15.
(40) Nakata, H.; Fedorov, D. G.; Nagata, T.; Yokojima, S.; Ogata, K.; Kitaura, K.; Nakamura, S. *J. Chem. Phys.* **2012**, *137*, 044110.
(41) Furche, F.; Ahlrichs, R. *J. Chem. Phys.* **2002**, *117*, 7433−7447.
(42) Nagata, T.; Fedorov, D. G.; Kitaura, K. *Chem. Phys. Lett.* **2010**, *492*, 302−308.
(43) Nakano, T.; Kaminuma, T.; Sato, T.; Fukuzawa, K.; Akiyama, Y.; Uebayasi, M.; Kitaura, K. *Chem. Phys. Lett.* **2002**, *351*, 475−480.
(44) Johnson, B. G.; Gill, P. M.; Pople, J. A. *J. Chem. Phys.* **1993**, *98*, 5612−5626.
(45) Schmidt, M. W.; Baldridge, K. K.; Boatz, J. A.; Elbert, S. T.; Gordon, M. S.; Jensen, J. H.; Koseki, S.; Matsunaga, N.; Nguyen, K. A.; Su, S.; et al. *J. Comput. Chem.* **1993**, *14*, 1347−1363.
(46) Fedorov, D. G.; Olson, R. M.; Kitaura, K.; Gordon, M. S.; Koseki, S. *J. Comput. Chem.* **2004**, *25*, 872.
(47) Fedorov, D. G.; Ishida, T.; Kitaura, K. *J. Phys. Chem. A* **2005**, *109*, 2638−2646.
(48) Fedorov, D. G.; Kitaura, K. *J. Chem. Phys.* **2004**, *120*, 6832−6840.
(49) Fedorov, D. G.; Kitaura, K. *Chem. Phys. Lett.* **2014**, *597*, 99−105.
(50) Pruitt, S. R.; Steinmann, C.; Jensen, J. H.; Gordon, M. S. *J. Chem. Theory Comput.* **2013**, *9*, 2235−2249.